Chapter 4

Scalogram-Based Gait Abnormalities Classification Using Deep Convolutional Networks for Neurological and Non-Neurological Disorders

Abstract

This chapter presents a methodology for classifying gait abnormalities utilizing convolutional neural networks (CNNs) and scalogram analysis of electromyography and foot insole data. Electromyography data was obtained from patients with conditions such as hemiplegia, rheumatoid arthritis, prolapsed intervertebral disc, and osteoarthritis. Additionally, foot insole data from the PhysioNet database included subjects with Parkinson's disease, Huntington's disease, and amyotrophic lateral sclerosis. The CNN-based classification tasks, optimized using various optimizers and pooling layers, exhibited high accuracy, with the adam optimizer and max pooling layer achieving a 96.75% accuracy rate for overall classification. In the case of four-class classification tasks, 96.62% and 96.96% accuracy were attained using adam and rmsprop optimizers with max pooling layers, respectively. These outcomes underscore the efficacy of the proposed methodology in precisely and consistently diagnosing gait abnormalities, implying its potential application in clinical settings for distinguishing between various gait disorders.

4.1 Introduction

To analyze and diagnose the gait of an individual, doctors and researchers mainly rely on data from modalities like Electromyography (EMG), Pressure Sensors, and Inertial Measurement Units (Singh et al., 2019). An assessment of the raw EMG plot and its envelope is helpful in the diagnosis of motor dysfunction. Analysis of EMG involves signal preprocessing (filtering, rectification, smoothing, and normalization), followed by statistical testing and computer algorithms (Konrad, 2005). In the present-day scenario, there is much emphasis on smart wearable devices to acquire diagnostic data, and one such device is the foot insole with an array of pressure sensors to measure the force exerted by the foot on the ground and finds application in gait data acquisition (Subramaniam et al., 2022).

4.2 Gait Abnormalities

Neuromuscular diseases cause muscle function and movement abnormalities that affect an individual's gait. Recognizing the characteristic alterations in gait patterns associated with these diseases aids in their early diagnosis (Volpe, 1988). Hence, gait analysis may be utilized for decision-making, diagnostics, and rehabilitation (Harris and Wertsch, 1994). The utilization of advanced gait analysis techniques in conjunction with the patient history and physical examination provides a thorough assessment of abnormalities (Baker, 2006). A routine assessment is generally carried out through a medication review, visual inspection, evaluation of basic activities of daily life, general gait parameter measurement, kinetic measurement, electromyography (EMG) assessment, and kinematic analysis (Whittle, 1996; Ganz et al., 2007).

Broadly gait abnormalities are divided into two categories, Neurological and non-neurological gait disorders (Alexander, 1996). Localized or widespread lesions cause

neurological gait disorders in the neural pathways connecting the cortical motor centers to the peripheral systems. Non-neurological gait abnormalities are often characterized by sluggish gait due to constraints caused by musculoskeletal, cardiac, or respiratory problems (Verghese et al., 2006). Some examples of neurologic gait abnormalities are those emerging due to sensory ataxia, hemiplegia, Parkinson's disease, frontal ataxia, and cerebral ataxia. Non-neurological gait mainly includes musculoskeletal ailments like osteoarthritis and skeletal deformities, and the main changes observed in gait are a decrease in range of motion and speed (Pirker and Katzenschlager, 2017). In recent years, the number of strokes has risen significantly. One of the significant consequences of a stroke is hemiplegia, which results in the paralysis of one side of the body (You and Chung, 2015). The signs of hemiplegia can vary depending on the extent of paralysis or weakness, but typical symptoms include paralysis or weakness on one side of the body and difficulty in movement or control of the affected limb (Hesse et al., 1997). Hemiplegic gait is characterized by a shorter stride and high swing phase ratios due to the unaffected leg compensating for the movement (McGee, 2021). Another condition affecting a large population is prolapsed intervertebral disc (PIVD), caused by disc displacement in the spine.

Major symptoms of PIVD are pain, numbness, weakness in the affected region, and antalgic gait (Kelsey, Golden, and Mundt, 1990; Humphreys and Eck, 1999). A common autoimmune condition in the middle-aged population is rheumatoid arthritis (RA) (McInnes and Schett, 2011). It causes joint and tissue inflammation leading to pain, stiffness, and trouble moving the afflicted joints. Gait characteristics of RA include antalgic gait, reduced walking speed, cadence, and stride length (Baan et al., 2012). Older people above the age of 60 often develop osteoarthritis, which is a degenerative joint condition in which the protecting cartilage on the ends of bones wears away over time, causing discomfort, stiffness, and swelling in joints, bone spurs, grating sensation, and difficulty

in movement (Broström et al., 2012; Hamerman, 1989). A severe neurodegenerative disease (NDD) that affects a large population is Parkinson's disease (PD). It impairs mobility and causes tremors, stiffness, and difficulties with balance and coordination (Mirelman et al., 2019). A Parkinsonian gait is characterized by jerking and freezing, decreased step length and speed, and increased cadence (Grabli et al., 2012). A rare but fatal genetic condition is Huntington's disease (HD) which causes nerve cell degeneration in the brain. Common symptoms include muscle spasms, cognitive impairment, and difficulty with speech. Bradykinesia and increased variability in spatiotemporal gait features are often observed in patients with HD (Vuong et al., 2018). Another rare neurodegenerative illness that damages the nerve cells regulating muscular movement is Amyotrophic Lateral Sclerosis (ALS). It causes muscular atrophy and trouble speaking, swallowing, and breathing leading to death. High variability in stride time and hypokinetic movement are characteristics of the gait of ALS patients (Moon et al., 2016).

4.3 Limitations of EMG

EMG allows for a comprehensive evaluation of muscle function and diagnoses neurological disorders by recording and analyzing the electrical activity of muscles. Despite having good classification accuracy, the EMG signal becomes weak in certain neuromuscular disorders and is insufficient for accurate classification of movement activity and, subsequently, for prosthetic device control. Another major challenge is its difficulty capturing complex and subtle movements in tasks requiring fine motor control (Enders and Nigg, 2016). Additionally, EMG signals can become unreliable over time due to muscle fatigue during prolonged activities (Dimitrova and Dimitrov, 2003). Invasive electrode placement can also be uncomfortable and present potential risks such as infection or tissue damage, limiting user acceptance (Uribe et al., 2010). Background noise is another factor that can impact EMG precision, especially for delicate movements (Boyer et al., 2023; Day, 2002).

In EMG, cross-talk results from signals from one muscle recording site being contaminated by electrical activity from neighboring muscles (Solomonow et al., 1994). Both techniques require careful electrode placement and signal processing techniques like filtering and source localization to reduce cross-talk (Mesin, 2018). Failure to address cross-talk can lead to misinterpretation of data and impact patient treatment and rehabilitation plans (Talib et al., 2019).

In EMG, inter-subject signal variability is primarily related to muscle structure, size, body composition, and motor control variations (Winter and Yack, 1987). These variations can affect the interpretation of muscle activity and assessment of neuromuscular disorders. Researchers establish baseline measurements for each individual or use normalized measures to compare muscle activity across different subjects (Guidetti et al., 1996). Clinicians also need to consider these natural differences when diagnosing conditions related to muscle function or evaluating the effectiveness of rehabilitation or physical therapy (Hug, 2011).

4.4 Wavelet Analysis and Scalograms

The continuous wavelet transform (CWT) is a powerful signal-processing technique with applications in various fields such as mathematics, computer science, and analytical chemistry. CWT is known for effectively handling distributed discontinuities (Kutyniok and Labate, 2008). It is an essential tool for dividing continuous-time functions into wavelets, providing a coherent framework for multiscale signal and image processing (Selesnick et al., 2005). The CWT has also been studied in the context of different transforms, further expanding its theoretical foundations and practical applications (Mandal et al., 2021; Pandey and Phukan, 2020).

Further, scalograms utilize CWT to convert 1D signal data into a 2D image format. This is particularly beneficial for deep learning-based classifiers like CNNs in image

classification (Phinyomark et al., 2011; Di Nardo et al., 2022). Specifically applied to Electromyography (EMG) data, scalograms prove adept at quantifying simulated muscle activity even in noisy conditions, proving invaluable in identifying gait abnormalities, such as those seen in Parkinson's disease (Romanato et al., 2021; Veer and Agarwal, 2014). In this study a methodology for classifying gait abnormalities using convolutional neural networks based on scalogram analysis of electromyography and foot insole data is proposed.

4.5 Materials and Methods

4.5.1 Dataset

The electromyography data from 50 participants was gathered from Sir Sunderlal Hospital (IMS), Varanasi, and various local clinics. The study received approval from the Institute Ethics Committee of the Institute of Medical Science (Banaras Hindu University), and consent was obtained from all participants. The participant group encompassed individuals with a range of conditions, including two with hemiplegia, one with prolapsed intervertebral disc (PIVD) of L4, L5, and S1 with rheumatoid arthritis, one with PIVD of L5, S1, and S2 along with piriformis syndrome, and another with PIVD accompanied by piriformis syndrome. Additionally, one participant had osteoarthritis. The participants' ages ranged from 25 to 69 years, with an average weight of (75 ± 12) kg and an average height of (166 ± 6) cm. EMG data from two major leg muscles, tibialis anterior (TA) and medial gastrocnemius (MGAS), were recorded using two Biometrics Ltd. DataLITE Wireless Surface EMG devices at a sampling frequency of 1000Hz. Participants were instructed to walk on level ground without support during the trials. The recorded data were processed using Python libraries, including Numpy, Pandas, PyWavelet, and SciPy. This involved filtering with a 20Hz to 450Hz bandpass filter, normalization, and rectifying the raw EMG

and vertical ground reaction force (vGRF) signals. Visual representations of the waveforms were generated using the matplotlib library. The complete procedure is detailed in Figure 4.1.

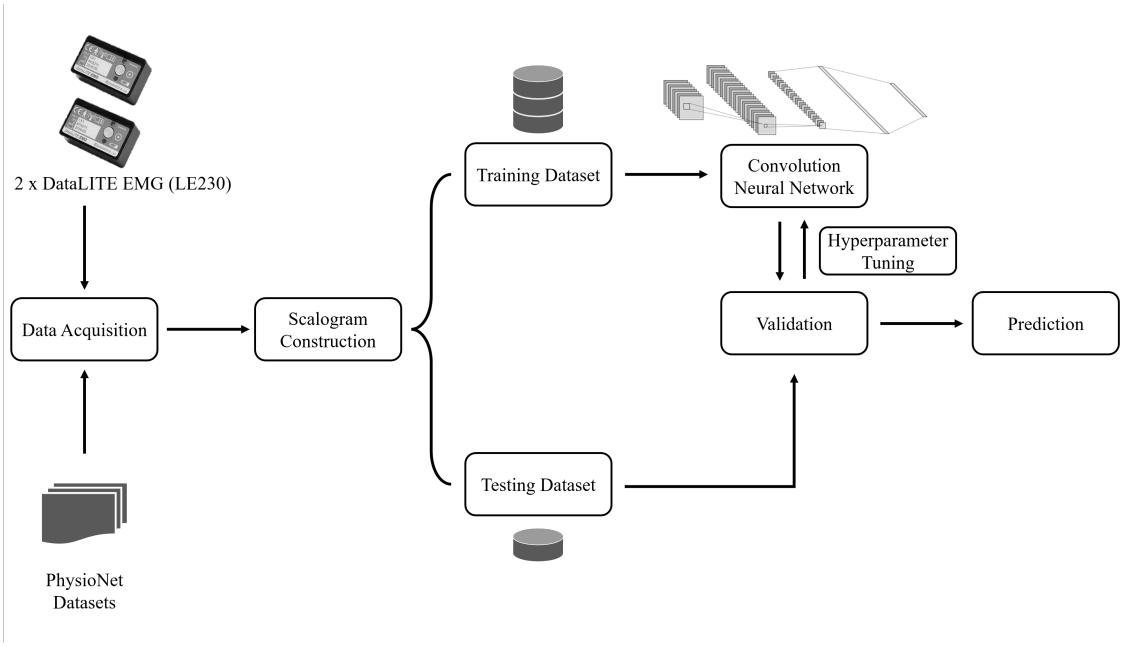

Fig. 4.1 Flowchart of the study

In addition, two publicly available datasets from PhysioNet (Goldberger et al., 2000) were used, which contain vGRF data obtained through foot insoles. The first dataset, gathered by Hausdorff et al. (2000), includes information from patients with three neurodegenerative conditions: Parkinson's disease (PD), Huntington's disease (HD), and amyotrophic lateral sclerosis (ALS). This dataset consists of 15 PD patients, 20 HD patients, 13 ALS patients, and 16 healthy individuals. The second dataset, compiled by Frenkel-Toledo et al. (2005), comprises vGRF data from 73 healthy participants and 93 individuals with Parkinson's disease, recorded using eight force sensors.

4.5.2 Feature Extraction

To better analyze the signal characteristics four time-domain features were also calculated using windowing technique. The four features used are Root Mean Square (RMS), Mean

Absolute Value (MAV), Skewness and Kurtosis. Table 4.1 provides information on the features used in the current study, where x represents the input sample, N represents the total number of samples, and μ represents the mean.

Table 4.1 EMG features used in the present study

Name	***Formula***	***Description***
MAV	$\frac{1}{N}\sum_{i=1}^{N}\|x_i\|$	The MAV can assess muscle activation during different tasks or movements.
RMS	$\sqrt{\frac{1}{N}\sum_{i=1}^{N}x_i^2}$	The RMS assesses muscle fatigue or changes in muscle activity over time.
Skewness	$\frac{1}{N}\sum_{i=1}^{N}\left(\frac{x_i-\mu}{\sigma}\right)^3$	Skewness assesses changes in muscle activity during different phases of a movement or task.
Kurtosis	$\frac{1}{N}\sum_{i=1}^{N}\left(\frac{x_i-\mu}{\sigma}\right)^4$	Kurtosis measures the muscle recruitment or coordination changes in the EMG signal distribution.

4.5.3 Scalogram Generation

The continuous wavelet transform (CWT) of a function *f(t)* is given by the convolution of *f(t)* with a scaled and a translated version of the wavelet function $\psi(t)$:

$$\mathrm{CWT}(a,b) = \frac{1}{\sqrt{|a|}}\int_{-\infty}^{\infty} x(t)\,\psi^*\left(\frac{t-b}{a}\right)dt \tag{4.1}$$

Where a is the scale factor and b is the translation factor.

Further, a scalogram is a graphical representation of the energy of a signal at different scales or frequencies and is often used in wavelet analysis to visualize the frequency content of a signal over time. Scalograms help identifies patterns and trends in a signal that may not be immediately apparent in the time domain (Arnal, 2014). The scalogram of the function representing energy at scale s is defined as:

$$S(a) = \|Wf(a,t)\| = \sqrt{\int_{-\infty}^{\infty}|Wf(a,t)|^2\,dt} \tag{4.2}$$

4.5.4 Deep Convolution Network

The scalogram images obtained constructed using the Mexican hat wavelet transform were further used in the Convolutional Neural network (CNN). CNN is a deep-learning neural network designed specifically for image recognition and processing (Lin and Lukodono, 2021). The three main layers of a CNN are the convolutional layer, pooling layers, and fully connected layers that make a prediction based on the extracted features (Li et al., 2021; Kim, 2017). Figure 4.2 shows a schematic of CNN used in the present study.

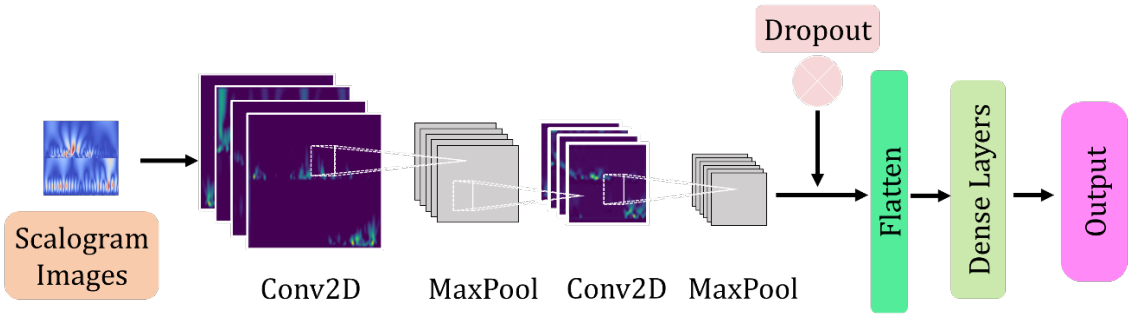

Fig. 4.2 Schematic diagram of a CNN

The scalogram images obtained for signal data were split into training and testing datasets with 75% of images used for training while 25% of images were used for testing. For EMG dataset 1500 images, for 4-class dataset 3012 images and, for 2-class dataset 1200 images were obtained. The Convolution Neural Network containing convolution, pooling, and dense layers was created using TensorFlow (Abadi et al., 2016). This study tested adam, stochastic gradient descent (SGD), and rmsprop optimizers as optimizer functions. As the pooling step is crucial in image transformation, CNNs with two different algorithms are trained: Max Pooling and Average Pooling. The comparison of the performance of the current model, was conducted using eight pre-trained models: VGG16, VGG19, ResNet50, Inceptionv3, InceptionResNet, MobileNet, MobileNetv2, DenseNet.

VGG16 and VGG19 are deep convolutional neural network architectures known for their simplicity and uniformity. They consist of multiple convolutional layers followed by

fully connected layers with a fixed input size. ResNet50 is a famous deep residual network architecture that introduced the concept of residual learning, utilizing skip connections to enable the training of very deep networks. Inceptionv3 and InceptionResNet are models that employ the inception module, which combines multiple filter sizes in parallel to capture information at different scales. MobileNet and MobileNetv2 are lightweight architectures designed for mobile and embedded devices, utilizing depth-wise separable convolutions to reduce computational complexity while maintaining performance. DenseNet introduces dense connectivity patterns, where each layer receives inputs from all preceding layers, promoting feature reuse and reducing the number of parameters. These models have been widely used in various computer vision tasks, including image classification and feature extraction, demonstrating their effectiveness and versatility.

4.6 Results and Discussion

The EMG waveforms obtained from the data are shown in Figure 4.3. It can be concluded that there is a significant effect on the gait pattern and general muscle activity. In some instances, it can be observed that one muscle seems to compensate for the lack of activity in another muscle. The jagged peaks in the said figure also point towards tremors and improper gait. Figure 4.4 shows waveforms of Healthy and Affected vGRF data for 4 class dataset, while Figure 4.5 shows the waveform for vGRF of both healthy subjects and subjects with Parkinson's disease.

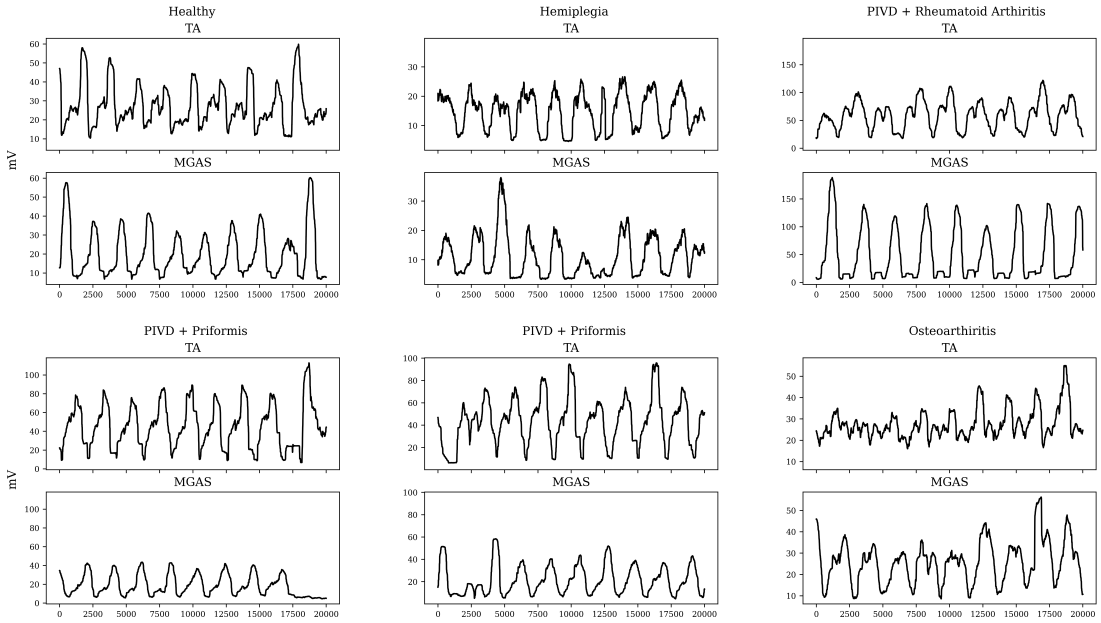

Fig. 4.3 EMG Signal Waveforms for each class

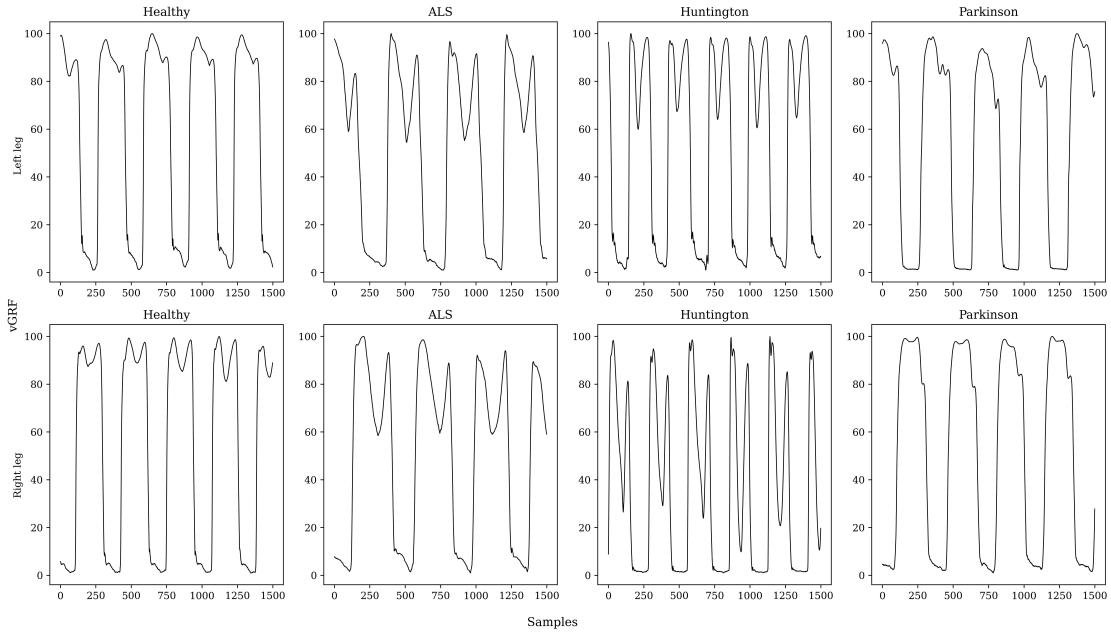

Fig. 4.4 vGRF Waveforms for Neurodegenerative disease dataset

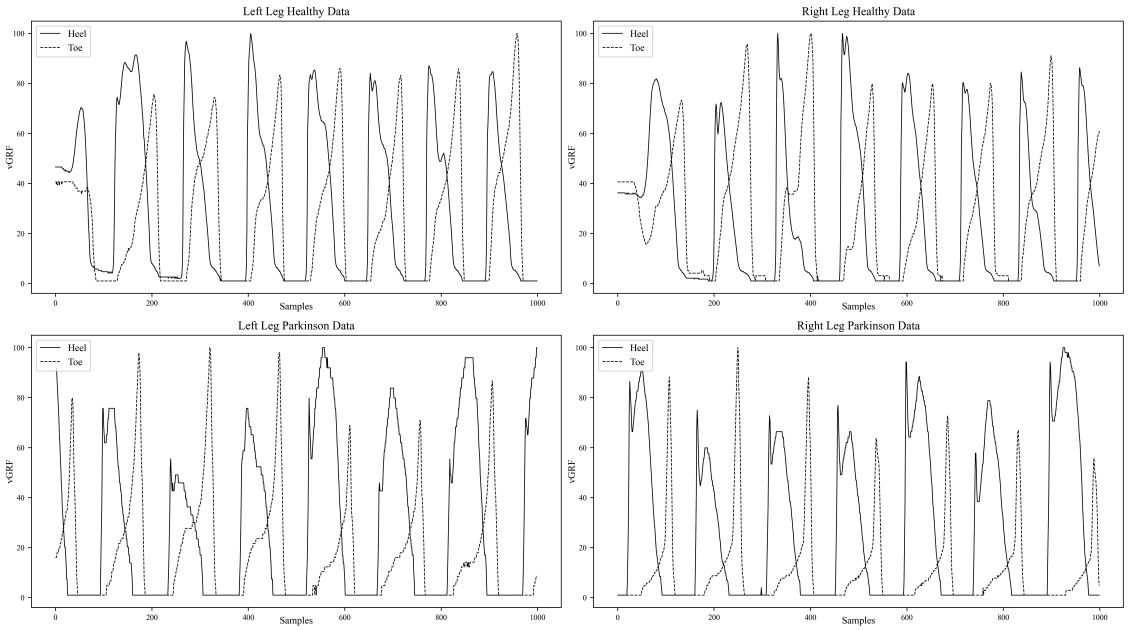

Fig. 4.5 vGRF Waveforms for Parkinson's disease dataset

Figure 4.6 shows a study of six EMG features for healthy individuals and those with Hemiplegia, RA, PIVD, and Osteoarthritis. The features examined include (a) root mean square (RMS), (b) mean amplitude values (MAV), (c) skewness, and (d) kurtosis. The first feature examined is root mean square (RMS), which shows a significant increase in affected muscles, particularly in RA, indicating heightened muscle recruitment and altered force production. The second feature, mean amplitude values (MAV), reveals elevated values in the tibialis anterior (TA) and medial gastrocnemius (MGAS) muscles, suggesting compensatory activity. However, interpretation considerations for factors like activity type and muscle fatigue are necessary. The third and fourth features, skewness, and kurtosis, highlight abnormal muscle activation patterns or reduced recruitment in neuromuscular disorders. The wavelet and scalogram analysis distinguish between a healthy subject and one with gait abnormality. Irregularities in the waveform of the latter also indicate muscle problems.

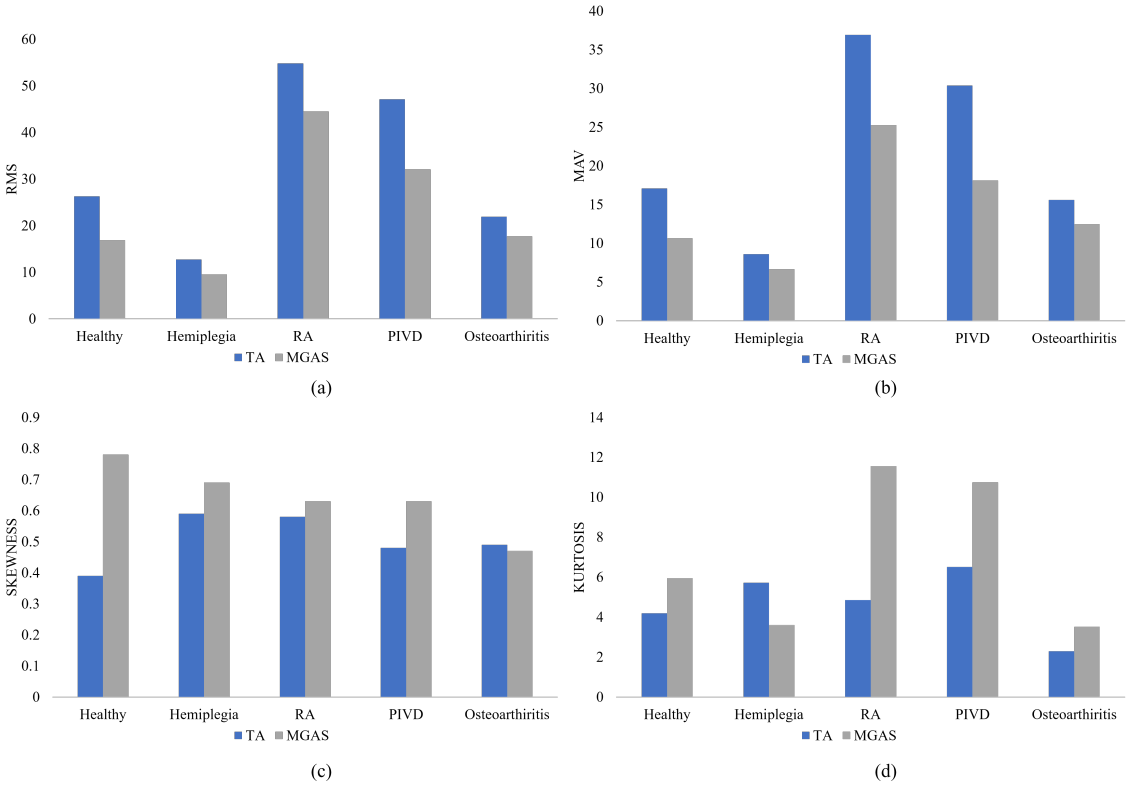

Fig. 4.6 Feature comparison of EMG signals. (a) RMS, (b) MAV, (c) Skewness, (d) Kurtosis

The generated wavelets are depicted in Figure with their corresponding scalograms. Figure 4.7(a) shows wavelet and scalogram for the healthy subject, while Figure 4.7(b) shows wavelet and scalogram for the subject with gait abnormality. It can be observed that there are signs of muscle problems in the second figure due to irregularities in the scalogram.

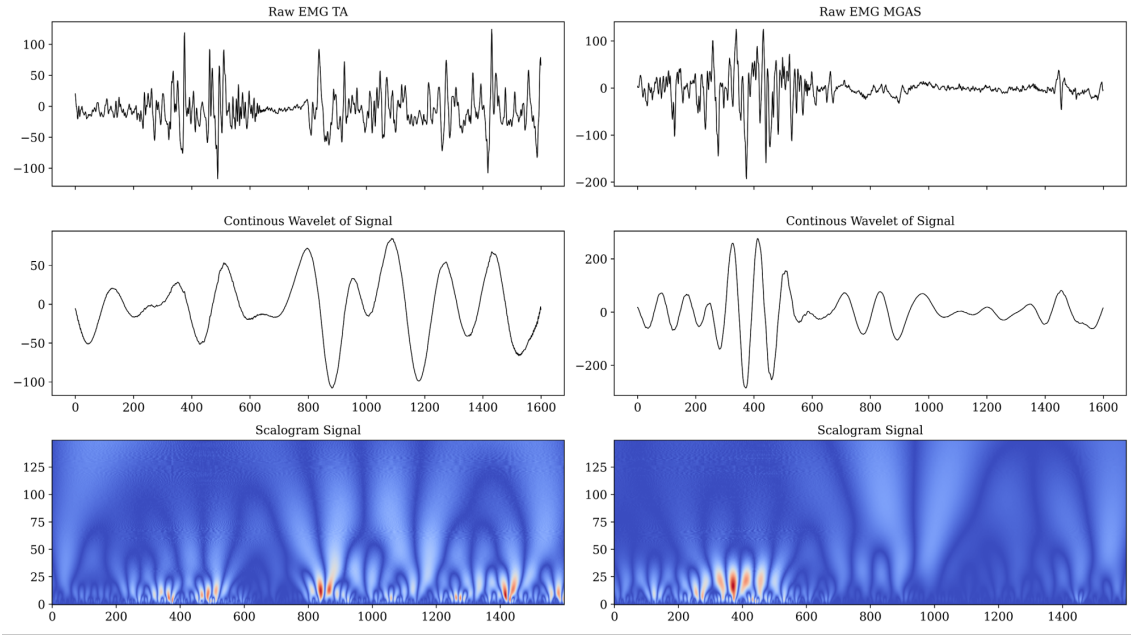

(a)

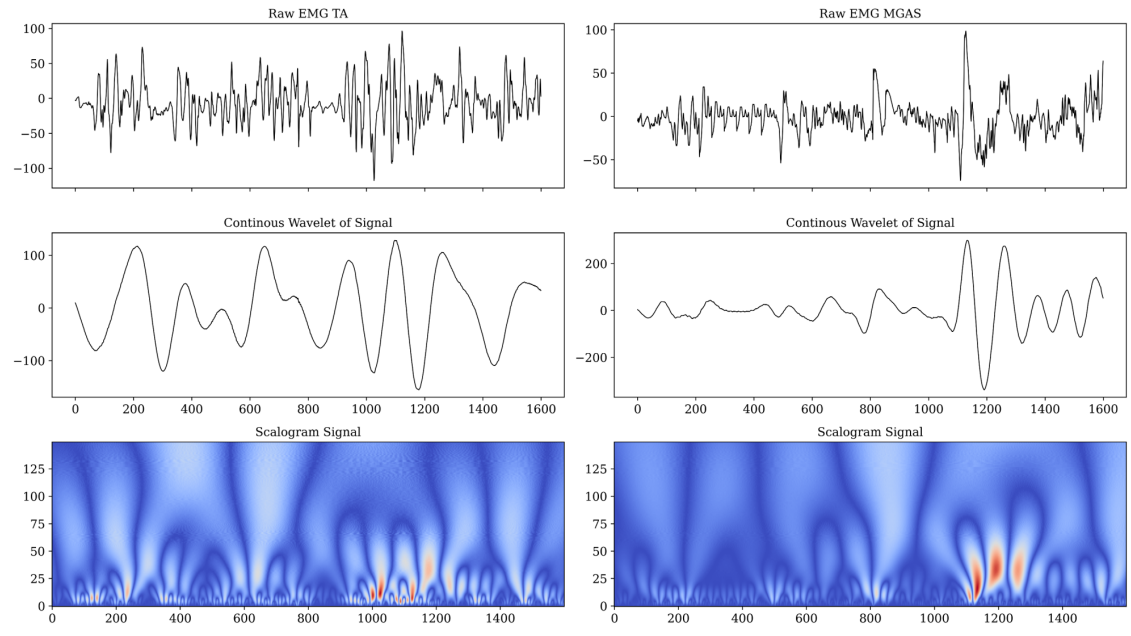

(b)

Fig. 4.7 Raw EMG signal, wavelet, and corresponding scalogram for (a) Healthy, (b) Affected

When utilizing the max pooling layer, the adam optimizer proved to be highly effective in minimizing loss, resulting in an impressive accuracy of 96.75%. Conversely, rmsprop and SGD exhibited suboptimal performance. The adam optimizer's achieved AUC score of 0.97 and a PRC of 0.94. Figure 4.8(a) Shows the loss value over 50 epochs for Max Pooling layers, while Figure 4.8(b) shows the loss value for the average pooling layer. Table 4.2 shows the various classification metrics for both CNNs.

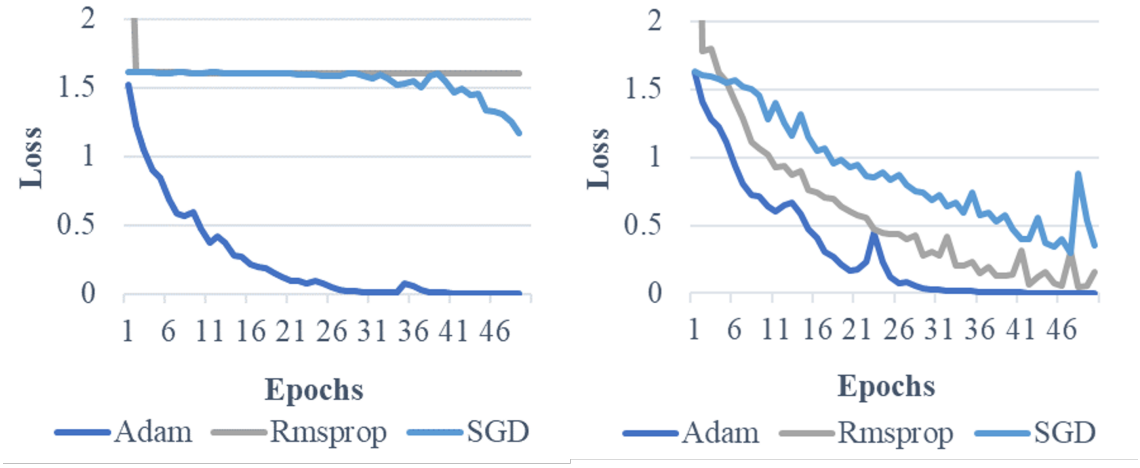

(a) (b)

Fig. 4.8 Comparison of optimizer performance for EMG data classification using (a) Max Pooling layers, and (b) Average pooling layers

Table 4.2 Classification accuracy for EMG dataset

	Max Pooling			**Average Pooling**		
	adam	*rmsprop*	*SGD*	*adam*	*rmsprop*	*SGD*
Accuracy	96.75%	80%	80.32%	95.70%	91.82%	87.16%
Precision	96.48%	48%	67.04%	96.59%	88.25%	84.15%
Recall	85.83%	37%	42.32%	80.30%	69.40%	63.86%
AUC	0.97	0.51	0.58	0.95	0.91	0.85
PRC	0.94	0.20	0.26	0.91	0.81	0.69

In four-class classification scenario, both adam and rmsprop optimizers achieved accuracies of 96.62% and 96.96%, respectively. These results were accompanied by AUC and PRC scores of 0.98 and 0.97, respectively. Figure 4.9(a) shows optimizer performances for four class dataset using max pooling layers. Table 4.3 shows the performance metrics. Figure 4.9(b) shows optimizer performances for average pooling layers.

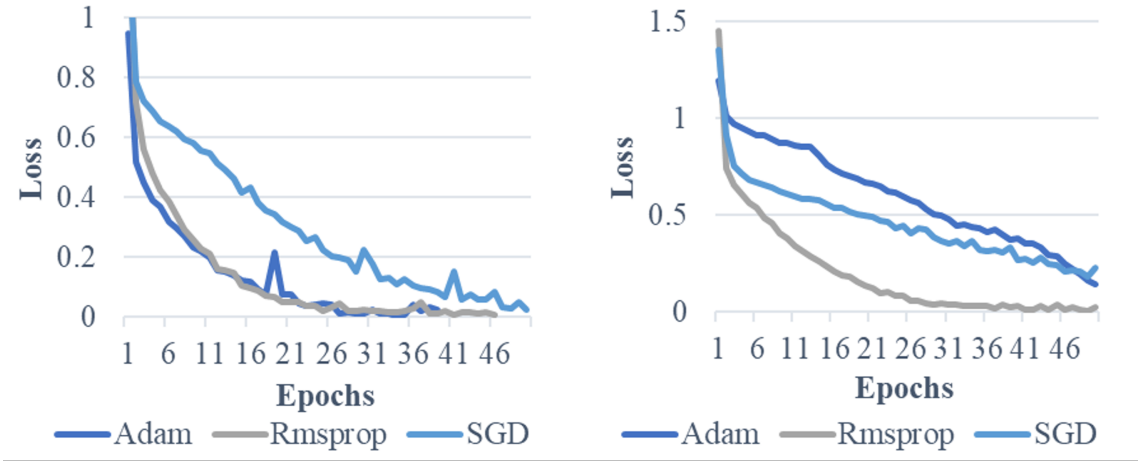

(a) (b)

Fig. 4.9 Comparison of optimizer performance for 4 class data classification using (a) Max Pooling layers, and (b) Average pooling layers

Table 4.3 Classification accuracy for four-class foot insole dataset

	Max Pooling			**Average Pooling**		
	adam	*rmsprop*	*SGD*	*adam*	*rmsprop*	*SGD*
Accuracy	96.62%	96.96%	93.44%	86.07%	95.86%	89.80%
Precision	93.69%	94.65%	89.32%	92.32%	92.67%	83.73%
Recall	92.32%	92.55%	82.85%	70.56%	89.86%	72.84%
AUC	0.98	0.98	0.97	0.91	0.98	0.95
PRC	0.97	0.97	0.92	0.80	0.95	0.88

When analyzing the two-class foot insole dataset, rmsprop emerged as the top-performing optimizer, achieving the highest accuracy rate of 88.13%. While this is a noteworthy result, the AUC and PRC scores of 0.91 suggest that there is room for refinement. Further optimization and extensive hyperparameter tuning may be necessary to unlock the full potential of the classifier in this two-class scenario. Figure 4.10 shows loss minimization for two class foot insole dataset, while Table 4.4 summarizes the classifier results. Rmsprop achieved the highest accuracy of 88.13% with an AUC and PRC of 0.91.

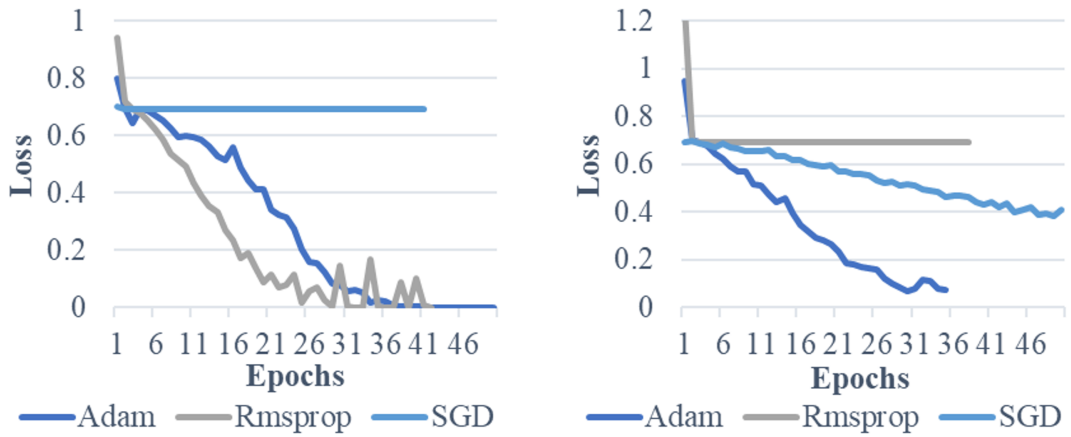

(a) (b)

Fig. 4.10 Comparison of optimizer performance for 2 class data classification using (a) Max Pooling layers, and (b) Average pooling layers

Table 4.4 Classification accuracy for two-class foot insole dataset

	Max Pooling			**Average Pooling**		
	adam	*rmsprop*	*SGD*	*adam*	*rmsprop*	*SGD*
Accuracy	84.57%	88.13%	50.45%	82.24%	50.59%	70.56%
Precision	86.07%	89.14%	50.67%	85.42%	45.43%	70.08%
Recall	83.35%	86.61%	66.27%	79.65%	83.05%	82.42%
AUC	0.88	0.91	0.48	0.87	0.49	0.76
PRC	0.89	0.91	0.49	0.88	0.50	0.79

Further, eight state-of-the-art architectures such as VGG16, VGG19, ResNet50, Inceptionv3, InceptionResNet, MobileNet, MobileNetv2, and DenseNet have been compared in this study. These models are widely used for various computer vision tasks including image classification and feature extraction. The study provides the performance evaluation of these models on three different datasets, which are EMG dataset, 4 class dataset, and 2 class datasets. The performance evaluation of the models on each dataset is presented in Figure 4.11, Figure 4.12, and Figure 4.13, respectively. The proposed model outperforms its competitors in both the 4-class and 2-class scenarios, as well as in EMG classification across various evaluation metrics. Its impressive balance between precision and recall makes it a powerful option for classification tasks.

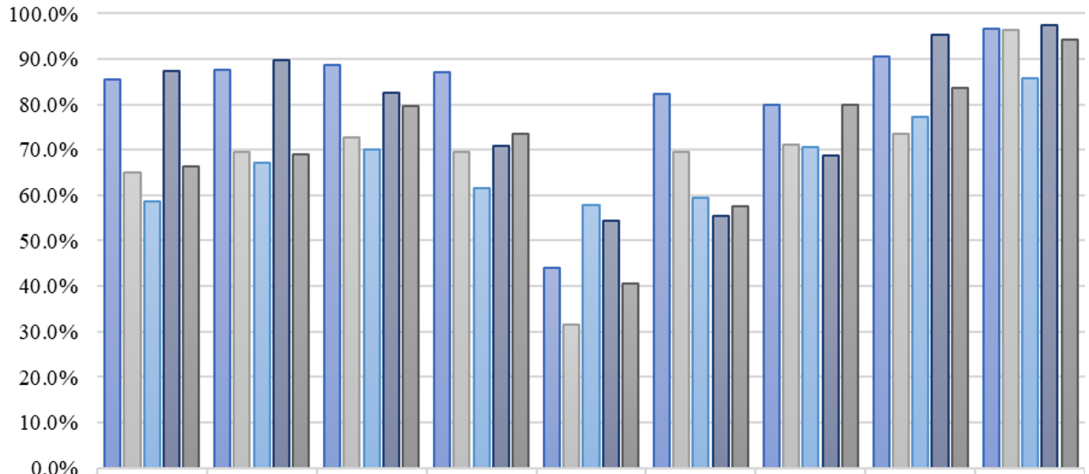

	VGG16	VGG19	ResNet	Inception	Inception-Resnet	Mobile Net	Mobile Net v2	DenseNet	Proposed
Accuracy	85.4%	87.5%	88.7%	87.0%	44.1%	82.2%	80.0%	90.4%	96.75%
Precision	64.9%	69.6%	72.7%	69.6%	31.6%	69.6%	71.1%	73.7%	96.48%
Recall	58.7%	67.1%	70.1%	61.7%	58.0%	59.5%	70.7%	77.4%	85.83%
AUC	0.8747	0.8966	0.8249	0.7084	0.5448	0.5546	0.6866	0.9541	0.9734
PRC	0.6642	0.691	0.7952	0.7345	0.4053	0.5759	0.7995	0.836	0.9432

Fig. 4.11 Comparison of proposed model with existing models for EMG classification

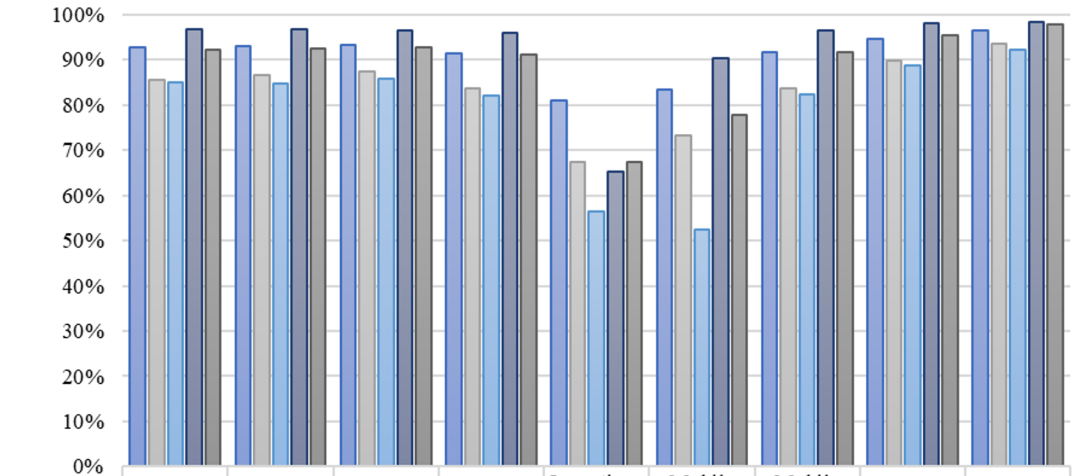

	VGG16	VGG19	ResNet	Inception	Inception-Resnet	Mobile Net	Mobile Net v2	DenseNet	Proposed
Accuracy	92.7%	92.9%	93.4%	91.5%	81.0%	83.3%	91.6%	94.7%	96.62%
Precision	85.7%	86.6%	87.5%	83.6%	67.4%	73.2%	83.8%	89.9%	93.69%
Recall	85.1%	84.8%	85.8%	82.1%	56.4%	52.5%	82.3%	88.8%	92.32%
AUC	0.9676	0.9673	0.9642	0.9608	0.6536	0.9024	0.9642	0.9813	0.9845
PRC	0.9214	0.9259	0.9282	0.912	0.6748	0.7768	0.9163	0.9541	0.9787

Fig. 4.12 Comparison of proposed model with existing models for 4 Class classification

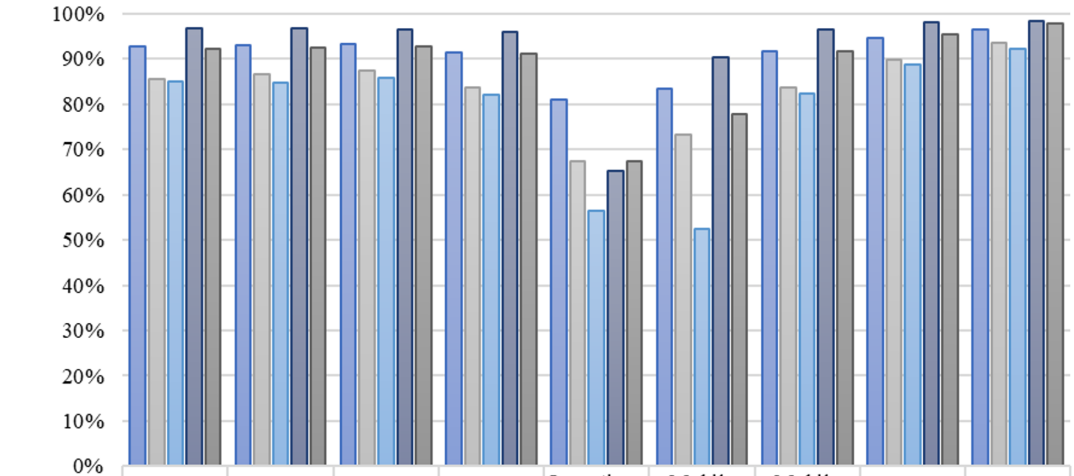

	VGG16	VGG19	ResNet	Inception	Inception-Resnet	Mobile Net	Mobile Net v2	DenseNet	Proposed
Accuracy	92.7%	92.9%	93.4%	91.5%	81.0%	83.3%	91.6%	94.7%	96.62%
Precision	85.7%	86.6%	87.5%	83.6%	67.4%	73.2%	83.8%	89.9%	93.69%
Recall	85.1%	84.8%	85.8%	82.1%	56.4%	52.5%	82.3%	88.8%	92.32%
AUC	0.9676	0.9673	0.9642	0.9608	0.6536	0.9024	0.9642	0.9813	0.9845
PRC	0.9214	0.9259	0.9282	0.912	0.6748	0.7768	0.9163	0.9541	0.9787

Fig. 4.13 Comparison of proposed model with existing models for 2 class classification

4.7 Conclusion

The classification of scalogram images from EMG and pressure data to detect gait abnormalities like hemiplegia, PIVD, RA, osteoarthritis, Parkinson's, Huntington's, and ALS was carried out using CNN. The classifier's performance was measured using accuracy, precision, recall, AUC, and PRC. The best accuracy of 96.75% for EMG classification was achieved using the Adam optimizer and max pooling layer, with an AUC and PRC of 0.97 and 0.94, respectively. Hence, it can be concluded that to correctly classify the changes in gait data occurring due to neurological and non-neurological factors, the application of a scalogram and CNN-based algorithm gives promising results and will be beneficial for doing diagnostics and rehabilitation plans.